DIHYDRINO MOLECULE IDENTIFICATION

RANDELL L. MILLS and WILLIAM R. GOOD
HydroCatalysis Power Corporation, Greenfield Corporate Center
1860 Charter Lane, Lancaster, Pennsylvania 17601

ROBERT M. SHAUBACH *Thermacore, Inc.*
780 Eden Road, Lancaster, Pennsylvania 17601

Received June 16, 1993
Accepted for Publication July 27, 1993

NUCLEAR REACTIONS IN SOLIDS

KEYWORDS: *calorimetry, mass spectroscopy, new hydrogen molecule*

Three sets of heat production and "ash" identification data are presented. An exothermic reaction is reported wherein the electrons of hydrogen and deuterium atoms are stimulated to relax to quantized potential energy levels below that of the "ground state" via electrochemical reactants K^+ and K^+; Pd^{2+} and Li^+; or Pd and O_2 of redox energy resonant with the energy hole that stimulates this transition. Calorimetry of pulsed current and continuous electrolysis of aqueous potassium carbonate (K^+/K^+ electrocatalytic couple) at a nickel cathode were performed. The excess output power of 41 W exceeded by a factor >8 the total input power given by the product of the electrolysis voltage and current. The product of the exothermic reaction is atoms having electrons of energy below the ground state, which are predicted to form molecules. The predicted molecules were identified by their lack of reactivity with oxygen, by separation from molecular deuterium by cryofiltration, and by mass spectroscopic analysis.

HYDROCATALYSIS POWER CORPORATION THEORY

Quantum mechanics based on the Schrödinger equation assumes that atomic-sized particles obey different physical laws than macroscopic objects, which behave classically. To overcome the shortcomings of quantum mechanics, physical laws that are exact on all scales were sought. Rather than endowing the electron with a wave nature as suggested by the Davisson-Germer experiment and fabricating a set of associated postulates and mathematical rules for wave operators, we derived a new theory from first principles. In both theories, solutions to the classical wave equation were sought, and the solution of the equation of the electron is time harmonic. But, the novel theory departs from the usual theory in the solutions of the spatial functions. Rather than invoking a postulated boundary condition, $\psi \to 0$ as $r \to \infty$, which leads to a purely mathematical model, we derived the boundary condition from Maxwell's equations[1]: *For nonradiative states, the charge-density function must not possess space-time Fourier components that are synchronous with waves traveling at the speed of light.*

Application of this physical boundary condition leads to a physical model that is consistent with classical physics. The novel theory[2] unifies Maxwell's equations, Newton's laws, and Einstein's general and special relativity. Theoretical predictions conform with experimental observations. The closed-form calculations of a broad spectrum of fundamental phenomena contain fundamental constants only. Equations of the one-electron atom are derived that give four quantum numbers, the Rydberg constant, the ionization energies, the results of the Stern-Gerlach experiment, the electron g factor, the spin angular momentum energies, the excited states, the results of the Davisson-Germer experiment, the parameters of pair production, and the hyperfine structure interval of positronium. Ionization energies of two- and three-electron atoms are given as well as the bond energies, vibrational energies, and bond distances of molecular hydrogen and the molecular hydrogen ion. From the closed-form solution of the helium atom, the predicted electron scattering intensity is derived. The closed-form scattering equation matches the experimental data, whereas calculations based on the Born model of the atom "utterly fail" at small scattering angles. The implications for the invalidity of the Schrödinger and Born models of the atom and the dependent Heisenberg uncertainty principle are discussed. The atomic equations of gravitation are derived from which the gravitational constant and the masses of the leptons and the neutron and proton are derived. The magnetic moments of the nucleons are derived. The beta decay energy of the neutron and the binding energy of deuterium are calculated. Also, the theory predicts exactly the spectral observations of the extreme ultraviolet background emission from interstellar matter, which characterizes dark matter; it

provides a resolution of the solar neutrino paradox, and it provides a basis to produce heat in electrolytic cells that represents an endless supply of cheap, clean energy.

A novel model of the electron[2] describes a bound electron by a charge-density (mass-density) function that is the product of a radial delta function [$f(r) = d(r - r_n)$], two angular functions (spherical harmonic functions), and a time-harmonic function. Thus, an electron is a spinning, two-dimensional spherical surface, called an electron orbitsphere, that can exist in a bound state only at specified distances from the nucleus.

PHOTON-INDUCED STATES OF THE ONE-ELECTRON ATOM

It is well known that resonator cavities can trap electromagnetic radiation of discrete resonant frequencies. A bound electron is a resonator cavity and can trap photons of discrete frequencies. The relationship between an allowed radius and the electron wavelength is

$$2\pi(nr_1) = 2\pi r_n = n\lambda_1 = \lambda_n \ , \tag{1}$$

where

$n = 1$

$n = 2,3,4, \ldots$

$n = \frac{1}{2}, \frac{1}{3}, \frac{1}{4}, \ldots$

λ_1 = allowed wavelength for $n = 1$

r_1 = allowed radius for $n = 1$.

Higher and lower energy states are equally valid. The photon standing wave in both cases is given as a solution of Laplace's equation in harmonic coordinates:

excited-state photon:

$$\hat{\epsilon i}_{r\,photon\,n,l,m} = \frac{e(na_0)^l}{4\pi\epsilon_0}\frac{1}{r^{(l+2)}} \times \left(-1 + \frac{1}{r}\,\mathrm{Re}\{i[Y_l^m(\phi,\theta) + Y_s^{m_s}(\phi,\theta)]\}\right) , \tag{2}$$

for

$$n = 2,3,4,\ldots,$$
$$l = 1,2,\ldots,n-1 \ ,$$

and

$$m_l = -l,-l+1,\ldots,0,\ldots,+l \ ;$$

below-ground-state photon:

$$\hat{\epsilon i}_{r\,photon\,n,l,m} = \frac{e}{4\pi\epsilon_0}\frac{\left(\frac{a_0}{n}\right)^l}{r^{(l+2)}} \times \{-1 + n[Y_l^m(\phi,\theta) + Y_s^{m_s}]\} \ , \tag{3}$$

for

$$n = 2,3,4,\ldots,$$

$$l = 1,2,\ldots,n-1 \ ,$$

and

$$m_l = -l,-l+1,\ldots,0,\ldots,+l \ .$$

From energy conservation, the resonance energy hole of a hydrogen atom that excites resonator modes of radial dimensions $a_0/(m+1)$ is

$$m \times 27.2 \text{ eV} \ ,$$

where

$$m = 1,2,3,4,\ldots \ .$$

After resonant absorption of the hole, the radius of the orbitsphere a_0 shrinks to $a_0/(m+1)$. After p cycles of resonant shrinkage, the radius is $a_0/(mp+1)$.

In other words, the radial ground-state field can be considered as the superposition of Fourier components. The removal of negative Fourier components of energy $m \times 27.2$ eV, where m is an integer, increases the positive electric field inside the spherical shell by m times the charge of a proton. The resultant electric field is a time-harmonic solution of LaPlace's equations in spherical coordinates. In this case, the radius at which force balance and nonradiation are achieved is $a_0/(m+1)$, where m is an integer. In the decay to this radius from the ground state, a total energy of $[(m+1)^2 - 1^2] \times 13.6$ eV is released. The potential energy well of the hydrogen or deuterium atom is shown in Fig. 1. The exothermic reaction is referred to as hydrogen emission by catalytic thermal electronic relaxation.

An efficient catalytic system that hinges on the coupling of three resonator cavities involves potassium. For example, the second ionization energy of potassium is 31.63 eV. This energy hole is obviously too high for resonant absorption. However, K^+ releases 4.34 eV when it is reduced to K. The combination of K^+ to K^{2+} and K^+ to K, then, has a net energy change of 27.28 eV:

$$27.28 \text{ eV} + K^+ + K^+ + H\left(\frac{a_0}{p}\right) \rightarrow K + K^{2+} + H\left[\frac{a_0}{(p+1)}\right] + [(p+1)^2 - p^2] \times 13.6 \text{ eV} , \tag{4}$$

$$K + K^{2+} \rightarrow K^+ + K^+ + 27.28 \text{ eV} . \tag{5}$$

And, the overall reaction is

$$H\left(\frac{a_0}{p}\right) \rightarrow H\left[\frac{a_0}{(p+1)}\right] + [(p+1)^2 - p^2] \times 13.6 \text{ eV} . \tag{6}$$

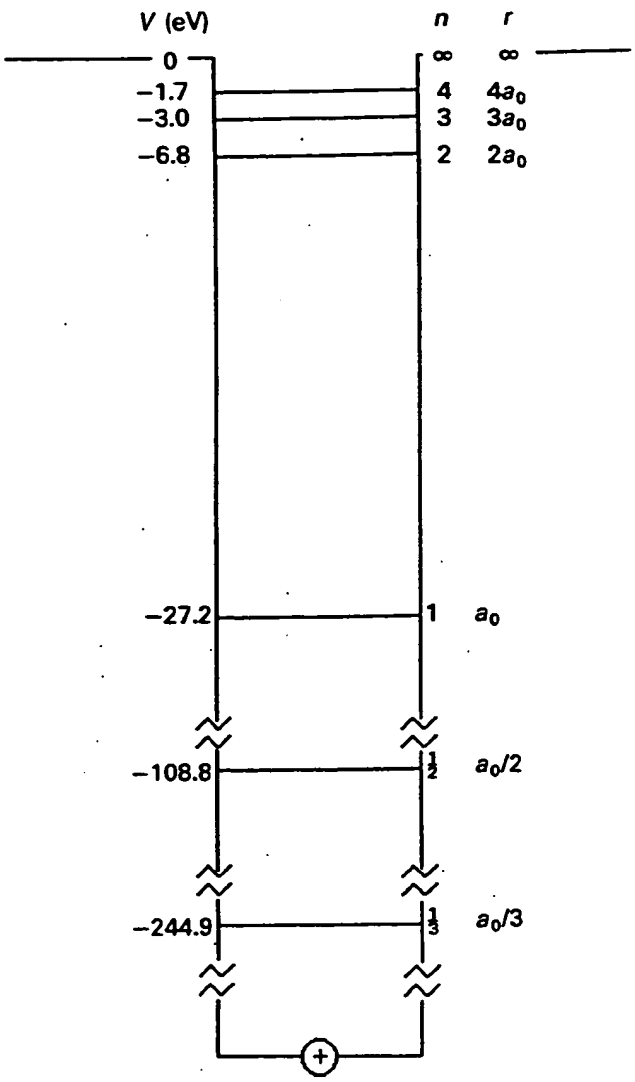

Fig. 1. Potential energy well of a hydrogen atom.

Other less efficient catalytic systems that hinge on the coupling of three resonator cavities exist. For example, the third ionization energy of palladium is 32.93 eV. This energy hole is obviously too high for resonant absorption. However, Li^+ releases 5.392 eV when it is reduced to Li. The combination of Pd^{2+} to Pd^{3+} and Li^+ to Li, then, has a net energy change of 27.54 eV:

$$27.54\ \text{eV} + Li^+ + Pd^{2+} + H\left(\frac{a_0}{p}\right) \rightarrow Li + Pd^{3+} + H\left[\frac{a_0}{(p+1)}\right] + [(p+1)^2 - p^2] \times 13.6\ \text{eV}\ , \quad (7)$$

$$Li + Pd^{3+} = Li^+ + Pd^{2+} + 27.54\ \text{eV}\ . \quad (8)$$

And, the overall reaction is

$$H\left(\frac{a_0}{p}\right) \rightarrow H\left[\frac{a_0}{(p+1)}\right] + [(p+1)^2 - p^2] \times 13.6\ \text{eV}\ . \quad (9)$$

A catalytic system that hinges on the transfer of two electrons from an atom to a molecule involves palladium and oxygen. For example, the first and second ionization energies of palladium are 8.34 and 19.43 eV, respectively, and the first and second electron affinities of the oxygen molecule are 0.45 and 0.11 eV, respectively. The energy hole resulting from a two-electron transfer is appropriate for resonant absorption. The combination of Pd to Pd^{2+} and O_2 to O_2^{2-}, then, has a net energy change of 27.21 eV:

$$27.21\ \text{eV} + Pd + O_2 + H\left(\frac{a_0}{p}\right) \rightarrow Pd^{2+} + O_2^{2-} + H\left[\frac{a_0}{(p+1)}\right] + [(p+1)^2 - p^2] \times 13.6\ \text{eV}\ , \quad (10)$$

$$Pd^{2+} + O_2^{2-} \rightarrow Pd + O_2 + 27.21\ \text{eV}\ , \quad (11)$$

And, the overall reaction is

$$H\left(\frac{a_0}{p}\right) \rightarrow H\left[\frac{a_0}{(p+1)}\right] + [(p+1)^2 - p^2] \times 13.6\ \text{eV}\ . \quad (12)$$

Additional atoms, molecules, or compounds that could be substituted for O_2 are those with first and second electron affinities of −0.45 and 0.11 eV, respectively, such as a mixed oxide (MnO_x, AlO_x, or SiO_x) containing oxygen to form O^{2-} or O_2 to form O_2^{2-}.

For sodium or sodium ions, no electrocatalytic reaction of −27.21 eV is possible. For example, 42.15 eV of energy is absorbed by the reverse of the reaction given in Eq. (5) where Na^+ replaces K^+:

$$Na^+ + Na^+ + 42.15\ \text{eV} \rightarrow Na + Na^{2+}\ . \quad (13)$$

NEW HYDROGEN MOLECULE

According to HydroCatalysis Power Company (HPC) theory, a hydrino atom, a hydrogen atom with its electron in a lower-than-ground-state energy level corresponding to a fractional quantum number, has an unpaired electron and would bind to the nickel cathode. Bound hydrogen atoms demonstrate a high degree of mobility as shown by electron energy loss spectroscopy.[3] Hydrino atoms are predicted to possess high mobility that permits the possibility of subsequent shrinkage reactions and dihydrino-molecule-forming reactions. The hydrino must form muon-like molecules, as indicated by the trace tritium production during the electrolysis of a K_2CO_3 heavy water electrolyte with a

nickel cathode.[2] Dihydrino molecules are evolved from the cathode and are found in the effluent electrolysis gas.

A preferred method to identify the dihydrino molecule is via cryofiltration followed by a search for mass spectroscopic anomalies.

EXISTING EVIDENCE FOR HYDRINO ATOMS AND DIHYDRINO MOLECULES

Hydrogen transitions to electronic energy levels below the $n = 1$ state have been found in the spectral lines of the extreme ultraviolet background of interstellar space. This assignment resolves the paradox of the identity of dark matter. It also accounts for other celestial observations such as the facts that diffuse Hα emission is ubiquitous throughout the galaxy and widespread sources of flux shortward of 912 Å are required to account for this emission.[2,4]

The dihydrino molecule can be identified by mass spectroscopy. Miles and coworkers[5-8] and Chien et al.[9] report ^{4}He production as identified by mass spectroscopy of the cryofiltered gases evolved from an electrolysis cell comprising a palladium cathode and a LiOD/D_2O electrolyte. According to Miles et al.,[7] the intensity of the helium peak maintained an approximate correspondence to the amount of excess power or heat observed in electrochemical calorimetric cells. The samples for helium analysis were analyzed "blindly" by mass spectroscopy. That is, the spectroscopist did not know whether a given sample produced excess heat or not.[10] According to Miles et al.,[7] "ignoring the helium/heat relationship (Table I of Ref. 7), the simple yes/no detection of helium in 7/7 experiments producing excess heat and the absence of helium in 6/6 experiments not producing excess heat (1 in D_2O, 5 in H_2O) implies a chance probability of $(\frac{1}{2})^{13} = \frac{1}{8192}$ or 0.012%." The fusion reaction proposed by the authors is as follows:

$$D + D \rightarrow {}^4He + \gamma(23.8\ MeV)\ . \qquad (14)$$

Miles et al.[8] report the production of ^{4}He at a rate of $\sim 10^{11}$ ^{4}He/s. The associated gamma emission from this proposed fusion corresponds to a 10-Ci 23.8-MeV source. Secondary X rays must also be present as well as neutrons and charged particles in the correct ratios.[11] No neutrons were observed, and no significant radiation above background was observed.[12] Numerous identical heat-producing experiments failed to produce fusion products within 13 orders of magnitude of that necessary to account for the heat.[13] According to Rees,[13] "even if a new fusion process were occurring, there ought to be x-rays produced. It is hard to believe that you could lose over 20 MeV in a single event and see nothing at all coming out."

We feel that the data are not consistent with a fusion reaction as the source of the excess heat or the mass 4 peak. The mass 4 peak is incorrectly assigned as ^{4}He. The correct assignment is D_2^*, the dideutrino molecule. These molecules form from deutrino atoms on the surface of the palladium cathode. The deutrino atoms form according to the exothermic reaction given by Eqs. (7), (8), and (9), which is the source of the observed excess heat.

The dideutrino molecule is predicted to be spin paired, to be of comparable size to the helium atom, and to have a higher ionization energy and a lower liquefaction temperature than D_2. Thus, cryofiltration of the gases of an electrolytic cell having an electrolyte of one or more electrocatalytic couples that induce transitions of deuterium atoms to energy levels below the ground state to release excess heat energy followed by mass spectroscopic analysis would appear to be producing ^{4}He. In fact, the mass spectroscopic separation of ^{4}He and D_2^* would be difficult. And, Miles et al.[10] used the higher ionization potential of the mass 4 peak as a criterion to make its assignment as ^{4}He rather than D_2.

The dideutrino molecule can also be identified by high-resolution quadrupole mass spectroscopy. Yamaguchi and Nishioka[14] reported high-resolution (0.001 amu) quadrupole mass spectroscopic data of the gases released from deuterium- or hydrogen-loaded palladium sheets coated on one side with a hydrogen-impermeable gold layer and coated on the other surface with an oxide coat (MnO_x, AlO_x, or SiO_x). Heat was observed from light and heavy hydrogen only when the mixed oxide coat was present. The mass spectroscopic data of the gases released when a current was applied to a deuterium-loaded (99.9%), MnO_x-coated palladium sheet indicate the presence of a large shoulder on the D_2 peak.

Yamaguchi and Nishioka's[14] control D_2 peak is shown in Fig. 2. A shoulder on the D_2 peak is shown in Figs. 3 (Ref. 14) and 4 (Ref. 15). The anomalous peak of Fig. 3 was assigned to HT (^{1}H-^{3}H) by Yamaguchi and Nishioka. Tritium is produced by nuclear fusion, and this (HT) peak grows with time as heat evolves. However, no such peak is possible because no ^{1}H was present, as demonstrated in the control spectrum, and the proposed HT peak was larger than the D_2 peak. The observed heat, including that observed from light hydrogen, is inexplicable from the proposed observed nuclear products. We assert that the data are not consistent with a fusion reaction or with the assignment of the anomalous mass 4 peak as HT. The correct assignment is D_2^*, the dideutrino molecule. These molecules form from deutrino atoms on the surface of the palladium sheet, and the deutrino atoms form according to the exothermic reaction given by Eqs. (10), (11), and (12), which is the source of the observed excess heat.

After cryofiltration or combustion, the dihydrino molecule can be distinguished from normal molecular hydrogen by mass spectroscopy. The branching ratio to form $m/e = 1$ relative to $m/e = 2$ that is observed for the dihydrino molecule is different than the ratio that

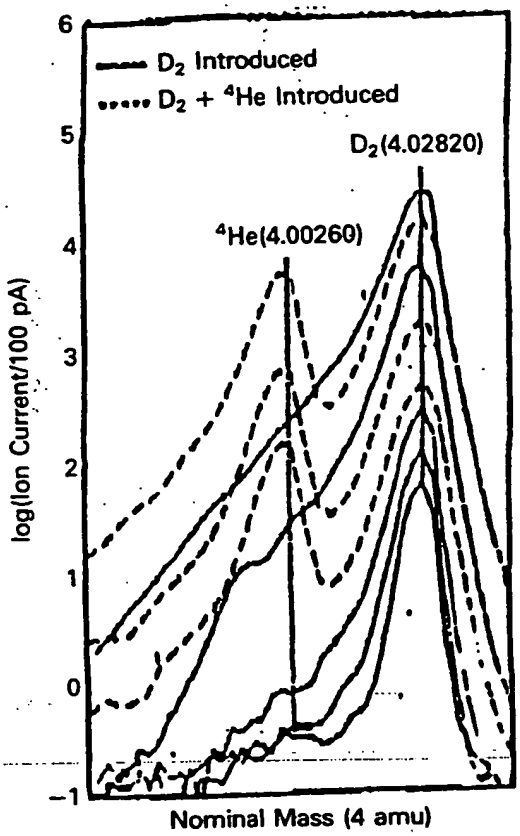

Fig. 2. Yamaguchi and Nishioka's[14] control high-resolution mass spectrum of helium and hydrogen.

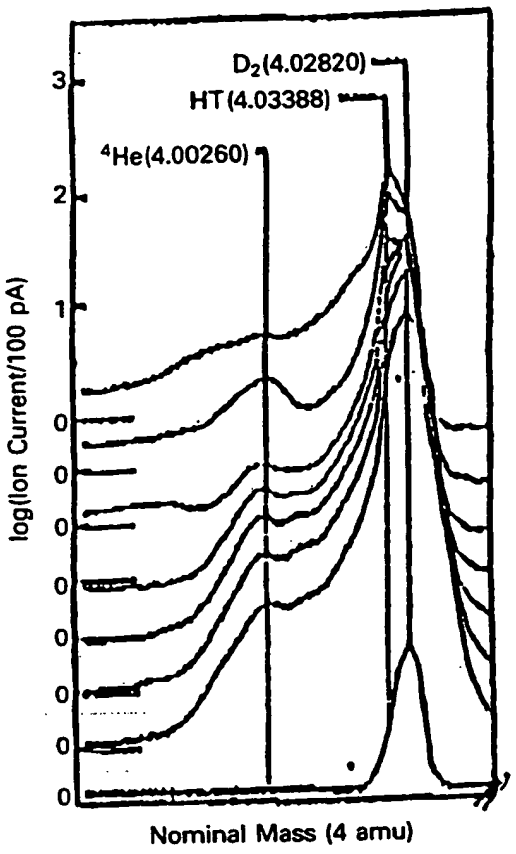

Fig. 3. Yamaguchi and Nishioka's[14] high-resolution mass spectroscopic data of the gases released when a current was applied to a deuterium-loaded (99.9%), MnO_x-coated palladium sheet, indicating the presence of a large shoulder on the D_2 peak that increases with time.

is observed for normal molecular hydrogen. Mass spectroscopy will further distinguish a sample containing dihydrino molecules from a sample containing H_2 by showing a different ion production efficiency as a function of ionization potential and a different ion production efficiency at a given ionization potential for the two samples.

LIGHT WATER CALORIMETRY EXPERIMENTS

Methods

A search for excess heat during the electrolysis of aqueous potassium carbonate (K^+/K^+ electrocatalytic couple) was conducted by using single-cell, silver-coated, vacuum-jacketed dewars and noninsulated plastic vessels. To simplify the calibration of these cells, they were constructed to have primarily conductive heat losses. Thus, a linear calibration curve was obtained. Two methods of differential calorimetry were used to determine the cell constant that was used to calculate the excess enthalpy. First, we calculated the cell constant during the experiment (on-the-fly calibration) by turning an internal resistance heater off and on and inferring the cell constant from the difference between the losses with and without the heater. Second, we determined the cell constant with no electrolysis processes occurring by turning an internal resistance heater off and on for a well-stirred cell and inferring the cell constant from the difference between the losses with and without the heater. This method overestimates the cell constant because there is no gas flow (which adds to the heat losses).

The general form of the energy balance equation for the cell in steady state is

$$0 = P_{appl} + Q_{htr} + Q_{xs} - P_{gas} - Q_{loss} , \qquad (15)$$

where

P_{appl} = electrolysis power

Q_{htr} = power input to the heater

Q_{xs} = excess heat power generated by the hydrogen "shrinkage" process

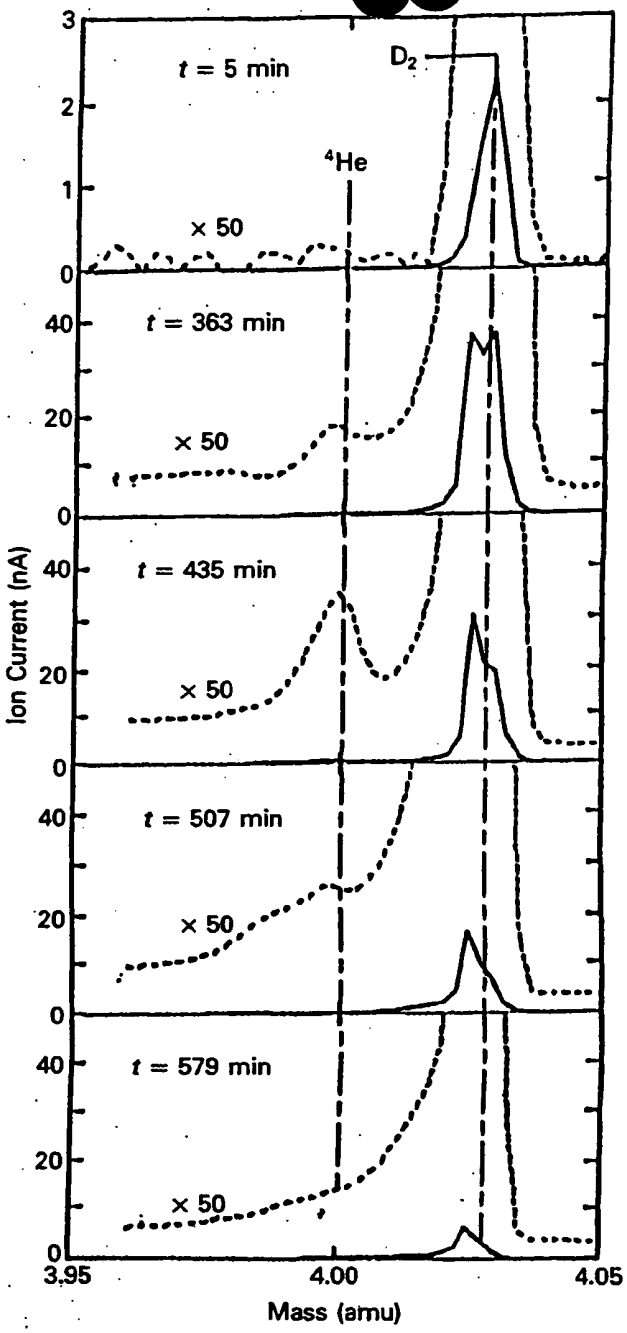

Fig. 4. Yamaguchi and Nishioka's[15] high-resolution mass spectroscopic data of the gases released when a current was applied to a deuterium-loaded (99.9%), MnO_x-coated palladium sheet, indicating the presence of a large shoulder on the D_2 peak that increases with time.

P_{gas} = power removed as a result of evolution of H_2 and O_2 gases

Q_{loss} = thermal power loss from the cell.

When an aqueous solution is electrolyzed to liberate hydrogen and oxygen gases, the electrolysis power P_{appl} ($= E_{appl}I$) can be partitioned into two terms:

$$P_{appl} = E_{appl}I = P_{cell} + P_{gas} \ . \tag{16}$$

An expression for P_{gas} ($= E_{gas}I$) is readily obtained from the known enthalpy of formation of water from its elements:

$$E_{gas} = \frac{-\Delta H_{form}}{\alpha F} \tag{17}$$

(F is Faraday's constant), which yields $E_{gas} = 1.48$ V for the reaction

$$H_2O \rightarrow H_2 + \tfrac{1}{2}O_2 \ . \tag{18}$$

The net faradaic efficiency of gas evolution is assumed to be unity; thus, Eq. (16) becomes

$$P_{cell} = (E_{appl} - 1.48V)I \ . \tag{19}$$

We calibrated the cell for heat losses by turning an internal resistance heater off and on while maintaining constant electrolysis and by inferring the cell conductive constant from the difference between the losses with and without the heater where heat losses were primarily conductive losses through the top of the dewar or through the surfaces of the plastic vessel. When the heater was off, the losses were given by

$$c(T_c - T_b) = P_{appl} + 0 + Q_{xs} - P_{gas} \ , \tag{20}$$

where

c = conductive heat loss coefficient

T_b = ambient temperature

T_c = cell temperature.

When a new steady state is established with the heater on, the losses change to

$$c(T'_c - T_b) = P'_{appl} + Q_{htr} + Q'_{xs} - P'_{gas} \ , \tag{21}$$

where the primes indicate values that changed when the heater was on. When we assume

$$Q_{xs} = Q'_{xs} \ , \quad P_{appl} = P'_{appl} \ , \quad \text{and} \quad P_{gas} = P'_{gas} \ , \tag{22}$$

the cell constant or heating coefficient a, the reciprocal of the conductive loss coefficient c, is given by the result

$$a = \frac{T'_c - T_c}{Q_{htr}} \ . \tag{23}$$

In all heater power calculations, we used the following equation:

$$Q_{htr} = E_{htr}I_{htr} \ . \tag{24}$$

In the case of intermittent square-wave electrolysis with current only during the high-voltage interval of the cycle, the P_{appl} value of Eq. (16) is calculated as the product of the peak voltage, the peak current, and the duty cycle Dc, which is the pulse length divided by the period:

$$P_{appl} = (E_{appl}I)Dc = (P_{cell} + P_{gas})Dc \ . \quad (25)$$

In the case of intermittent square-wave electrolysis with current only during the high-voltage interval of the cycle and where the net faradaic efficiency of gas evolution is assumed to be unity, P_{cell} of Eq. (19) becomes

$$P_{cell} = [(E_{appl} - 1.48V)I]Dc \ . \quad (26)$$

HPC Experiments 1, 2, and 3

These experiments were carried out by observing and comparing the temperature differences, $\Delta T_1 = T$(electrolysis only) $- T$(blank) and $\Delta T_2 = T$(resistor heating only) $- T$(blank) referred to unit input power, between two identical cells. Each cell consisted of a 350-ml silver-coated, vacuum-jacketed dewar (Cole Palmer model 8600) with a 7-cm opening covered with a 0.75-in.-thick Styrofoam stopper lined with Parafilm. One calorimeter dewar of the same configuration, containing the same amount of electrolyte and the same electrodes (nickel cathode and platinum anode), resistor-heater, and thermistor, stirred at the same speed, was used as the blank. In this dewar, neither electrolysis nor heating by the resistor was carried out. Experiments were also carried out by using the blank dewar from a previous experiment as the working dewar and vice versa. This exchange was done to ensure that the effect is not due to any difference in the thermal properties of the two specific dewars used. The experimental apparatus for the differential calorimetry used for these studies is shown in Fig. 5.

The heating coefficients were calculated from

$$a = \Delta T_1 / P_{cell} \quad (27)$$

and

$$a = \Delta T_2 / Q_{htr} \ . \quad (28)$$

The outsides of the cells were maintained at ambient air temperature, which was monitored. Ambient temperature fluctuations over 24 h were typically <0.5°C.

The cathode was 24 m of 0.127-mm-diam nickel wire (99% Alfa 10249, cold drawn) that was coiled about the central platinum anode. We cleaned the cathode by placing it in a beaker of 0.57 M K_2CO_3/3% H_2O_2 for 30 min and then rinsing it with distilled water. The leads were inserted into Teflon tubes to ensure that no recombination of the evolving gases occurred.

The anode was a 10-cm × 1-mm-diam spiraled platinum wire (Johnson-Matthey) with a 0.127-mm platinum lead wire. The leads were inserted into Teflon tubes to prevent recombination, if any, of the evolving gases. The cathode-anode separation distance was 1 cm.

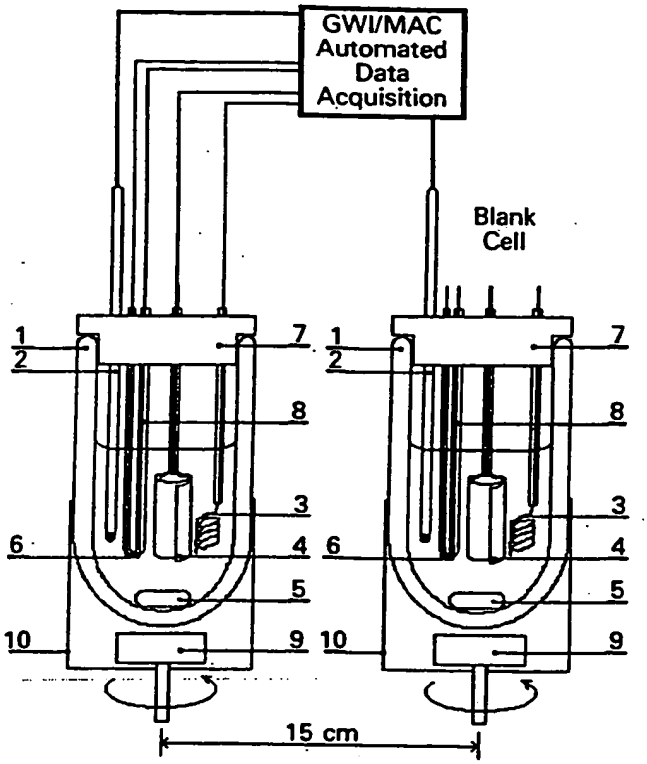

Fig. 5. Experimental calorimeter setup: (1) vacuum-jacketed dewar, (2) thermistor, (3) platinum anode, (4) nickel cathode, (5) magnetic stirring bar, (6) resistor-heater, (7) Styrofoam stopper lined with Parafilm, (8) Teflon tubing, (9) magnetic stirrer, and (10) aluminum cylinder.

As usual in electrochemistry, measures were taken to avoid impurities in the system, especially organic substances. We note here the known problems with the reproducibility of the hydrogen overpotential that can be overcome only by ensuring the lowest possible level of impurities. The following procedures were applied in order to reproduce the excess heat effect. Before starting the experiment, the electrolysis dewar was cleaned with Alconox and 0.1 M nitric acid and rinsed thoroughly with distilled water to remove all organic contaminants. The platinum anode was mechanically scoured with steel wool, soaked overnight in concentrated HNO_3, and rinsed with distilled water. The nickel cathode was removed from its container with rubber gloves, and cut and folded in such a way that no organic substances were transferred to the nickel surface. The nickel cathode was dipped into the working

solution under electrolysis current and was never left in the working solution without electrolysis current.

In experiments 1 and 2, the electrolyte solution was 200 ml of 0.57 *M* aqueous K_2CO_3 (Aldrich $K_2CO_3 * \frac{3}{2}H_2O$ 99+%); in experiment 3, the electrolyte solution was 200 ml of 0.57 *M* aqueous Na_2CO_3 (Aldrich Na_2CO_3 ACS primary standard 99.95+%).

The resistance heater used during calibration and operation was a 10-Ω, 1% precision metal oxide resistor in a 2-mm-o.d. Teflon tube. The heater was powered by a variable direct current voltage power source (±0.5%). The heating power was calculated by Eq. (24).

The electrolyte solution was stirred with a 7-mm × 2-cm prolate spheroid magnetic stirring bar that was spun by a 6-cm-long open magnet mounted on an open shaft revolving at 750 rpm under the dewar. The shaft was that of an open mixing motor (Fisher Flexa-Mix model 76).

Erroneous attribution of the effect to temperature gradients was prevented by testing for minute spatial variations of the temperature over time. Three thermistors were positioned ~2.5 cm apart from each other at the bottom, middle, and upper parts of the electrolyte. No difference was observed (within the limit of detection, ±0.01°C).

Voltage (±0.5%), current (±1%), and temperature (±0.1°C) data were acquired by a data acquisition system consisting of an Apple Mac II SI 5/80 with an NU bus adapter and the following GW Instruments hardware: GWI-625 data acquisition board, GWI-J2E multiplexer, GWI-ABO analog breakout system, and GWI-4W ribbon cable. The value of P_{appl} was given by Eq. (16) as the product of the voltage and the constant current, and P_{cell} was given by Eq. (19).

The current voltage parameters for experiment 2 were a periodic square wave having an offset voltage of 1.60 V, a peak voltage of 1.90 V, a peak constant current of 47.3 mA, a 36.0% duty cycle, and a frequency of 600 Hz. Peak voltage measurements were made with an oscilloscope (BK model 2120), and the time-average current was determined from a multimeter voltage measurement (±0.5%) across a calibrated resistor (1 Ω) in series with the lead to the cathode. The waveform of the pulsed cell was a square wave. Since there was current only during the peak voltage interval of the cycle, P_{appl} was given by Eq. (25), and P_{cell} was given by Eq. (26).

The faradaic efficiency of gas production by a potassium cell was studied. Comparing this result with the sodium system allows the accuracy of the analysis to be seen. A closed cell was fashioned from a 150-ml round-bottom flask, a 2-cm × 2-mm prolate spheroid stir bar, a glass "Y" adapter, glass tubing bent into the shape of one cycle of a square wave, a 150-ml beaker, and a 0.01-ml graduated buret. The cell was set up to mimic the calorimetry tests as closely as possible. A constant current (±0.1%) supply was used to supply the power for the electrolysis. Current measurement was done with a Heathly multimeter (±0.1%). Gas was collected and measured in the buret. Several experiments were run to ensure that the cell was sealed tightly.

Thermacore Experiment 4

The cell was a 10-gal (33- × 15-in.) Nalgene tank (model 54100-0010). Two 4-in.-long × $\frac{1}{2}$-in.-diam terminal bolts were secured in the lid, and a cord for a calibration heater was inserted through the lid.

The cathode was a 5-gal polyethylene bucket with $\frac{1}{2}$-in. holes drilled over all surfaces at $\frac{3}{4}$-in. spacings of the hole centers, which served as a perforated (mesh) support structure, and 5000 m of 0.5-mm-diam clean, cold-drawn nickel wire (NI 200, 0.0197-in., HTN36-NOAG1, A1 Wire Tech). The wire was wound uniformly around the outside of the mesh support as 150 sections of 33-m length. The ends of each of the 150 sections were spun to form three cables of 50 sections per cable. The cables were pressed in a terminal connector that was bolted to the cathode terminal post. The connection was covered with epoxy to prevent corrosion. A central cathode was made from 5000 m of the 0.5-mm-diam nickel wire. The wire was wound in a toroidal shape with three cables, each pressed into a terminal connector that was bolted to the cathode terminal post and coated with epoxy. The central cathode was inserted into an cylindrical perforated polyethylene container that was placed inside the outer cathode with the anode array between the central and outer cathodes.

The anode was an array of 15 platinized titanium anodes (ten of Engelhard platinum-titanium mesh, 1.6 × 8 in., with a $\frac{3}{4}$- × 7-in. stem attached to the 1.6-in. side plated with 100 U series 3000; and five of Engelhard 1-in.-diam × 8-in.-long titanium tubes with a $\frac{3}{4}$- × 7-in. stem affixed to the interior of one end and plated with 100 U platinum series 3000). A $\frac{3}{4}$-in.-wide tab was made at the end of the stem of each anode by bending it at a right angle to the anode. A $\frac{1}{4}$-in. hole was drilled in the center of each tab. The tabs were bolted to a 12.25-in.-diam polyethylene disk (Rubbermaid JN2-2669) equidistantly around the circumference. Thus, an array was fabricated that had 15 anodes suspended from the disk. The anodes were bolted with $\frac{1}{4}$-in. polyethylene bolts. Sandwiched between each anode tab and the disk was a flattened nickel cylinder also bolted to the tab and the disk. The cylinder was made from a 7.5- × 9-cm-long × 0.125-mm-thick nickel foil. The cylinder traversed the disk, and the other end of each was pressed about a 10 AWG/600 V copper wire. The connection was sealed with shrink tubing and epoxy. The wires were pressed into two terminal connectors and bolted to the anode terminal. The connection was covered with epoxy to prevent corrosion.

Before assembly, the anode array was cleaned in 3 *M* HCl for 5 min and rinsed with distilled water. The cathode was placed in a tank of 0.57 *M* K_2CO_3/3% H_2O_2 for 6 h and then rinsed with distilled water. The anode was placed in the support between the central

and outer cathodes, and the electrode assembly was placed in the tank containing 28 ℓ of 0.57 M K_2CO_3 (Alfa K_2CO_3 99%). The power supply was connected to the terminals with battery cables.

The cell assembly is shown in Fig. 6.

The heater was a 57.6-Ω, 1000-W Incoloy 800–jacketed Nichrome heater that was suspended from the polyethylene disk of the anode array. It was powered by a constant power (±0.1%) supply (Invar model TP 36-18). The voltage (±0.1%) and current (±0.1%) were recorded with a digital multimeter (Fluke 8600A). The current (±0.5%) was read from an Ohio Semitronics CTA 101 current transducer. The heating power was calculated by using Eq. (24).

Electrolysis was performed at 50-A constant current with a constant current (±0.02%) power supply (Kepco model ATE6-100M). The value of P_{appl} was given by Eq. (16) as the product of the voltage and the constant current, and P_{cell} was given by Eq. (19).

The temperature (±0.1°C) was recorded with a microprocessor thermometer (Omega HH21) using a type K thermocouple that was inserted through a $\frac{1}{4}$-in. hole in the tank lid and anode array disk. To eliminate the possibility of temperature gradients, the temperature was measured throughout the tank. No position variation was found to within the detection of the thermocouple (±0.1°C).

The temperature rise above ambient [$\Delta T = T$(electrolysis only) − T(blank)] and electrolysis power were recorded daily. The heating coefficient was determined on the fly by the addition of 20 W of heater power to the electrolytic cell every 72 h; 24 h was allowed for steady state to be achieved. The temperature rise above ambient [$\Delta T_2 = T$(electrolysis + heater) − T(blank)] was recorded as were the electrolysis power and heater power.

In all temperature measurements, the blank consisted of 28 ℓ of water in a 10-gal (33- × 15-in.) Nalgene tank with lid (model 54100-0010). The stirrer was a 1-cm-diam × 43-cm-long glass rod to which an 0.8- × 2.5-cm Teflon half-moon paddle was fastened at one end; the other end was connected to a variable-speed stirring motor (Talboys Instrument model 1075C). The stirring rod was rotated at 250 rpm.

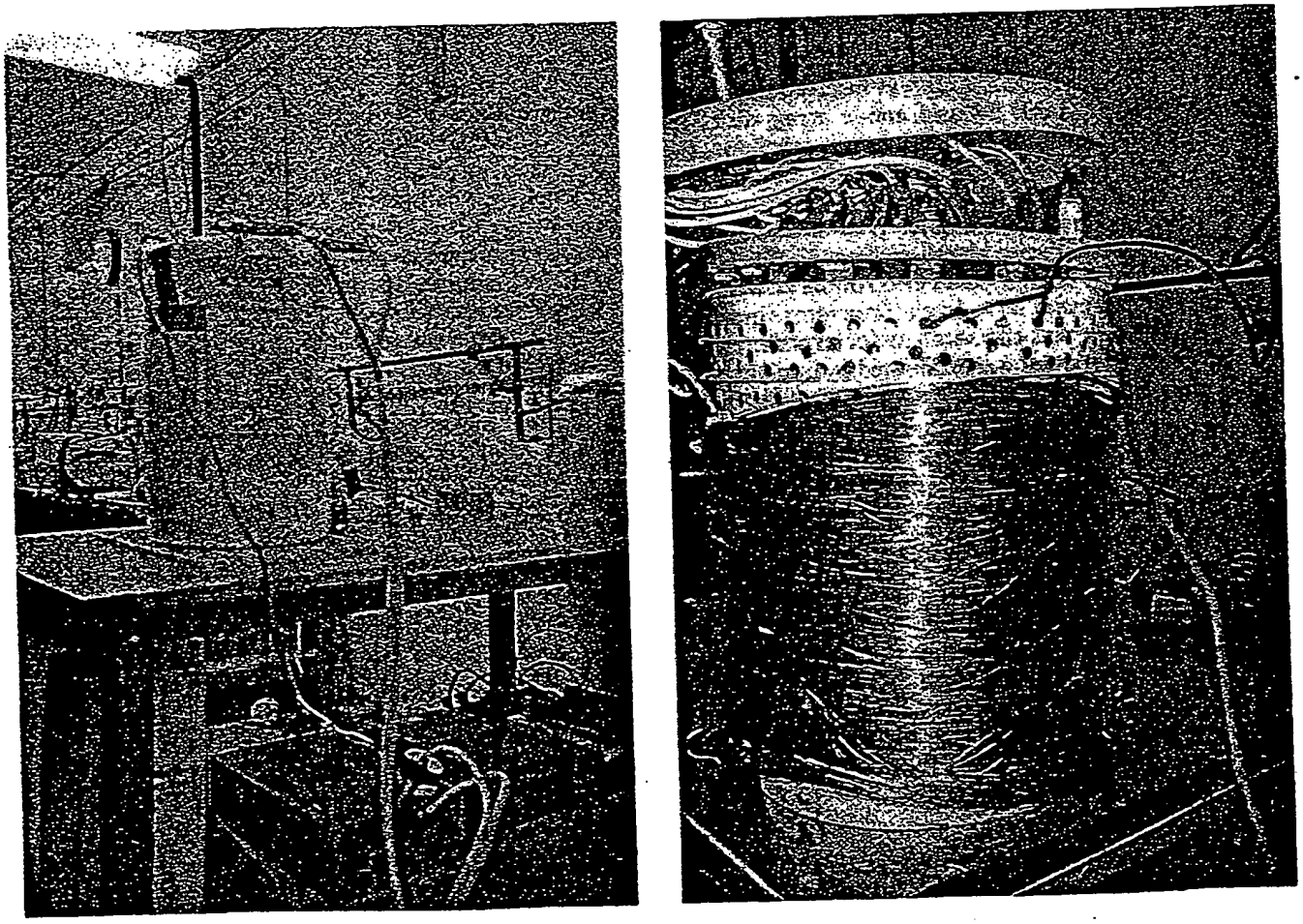

Fig. 6. Cell assembly of experiments 4 through 14.

The blank (nonelectrolysis cell) was stirred to simulate stirring in the electrolytic cell by gas sparging. The 1 W of heat from stirring resulted in the blank cell operating at 0.2°C above ambient.

The temperature (±0.1°C) of the blank was recorded with a microprocessor thermometer (Omega HH21) that was inserted through a $\frac{1}{4}$-in. hole in the tank lid.

Thermacore Experiments 5 Through 13

The electrolytic cell was the same as in experiment 4. Intermittent square-wave electrolysis was performed at 2 Hz at the duty cycles listed in Table I. A constant current supply (Kepco ATE-100M) was programmed at 101-A peak current (±0.05%) and driven by a function generator (BK Precision Dynascan model 3011). Duty cycle measurements were made with an oscilloscope (BK model 2120), and the peak current was determined from the voltage measurement (±0.1%) across an Ohio Semitronics CTA 101 current transducer. The waveform of the pulsed cell current was a square wave. Since there was current only during the peak voltage interval of the cycle, P_{appl} was given by Eq. (25), and P_{cell} was given by Eq. (26).

The peak voltage (±0.1%) was recorded with a digital multimeter (Fluke 8600A). The temperature (±0.1°C) was recorded with a microprocessor thermometer (Omega HH21) that was inserted through a $\frac{1}{4}$-in. hole in the tank lid and anode array disk. To eliminate the possibility of temperature gradients, the temperature was measured throughout the tank. No position variation was found to within the detection limit of the thermocouple (±0.1°C).

The temperature rise above ambient [$\Delta T = T$(electrolysis only) − T(blank)] and electrolysis power were recorded at least every 24 h. In all temperature measurements, the blank was the same as for experiment 4.

The electrolytic cell was calibrated by applying electrical power to the 1000-W heater with electrolysis power set to near zero. The cell temperature rise above ambient [$\Delta T = T$(heater only) − T(blank)] and heater power were recorded daily. The heating coefficient was determined on the fly by the addition of 40 W of heater power every 72 h; at least 24 h was allowed for steady state to be achieved. The heating power was calculated by Eq. (24).

TABLE I

Duty Cycles for Experiments 5 Through 13

Experiment	Duty Cycle (%)
5	3
6	4
7	5
8	6
9	7
10	10
11	15
12	20
13	25

Thermacore Experiment 14

The electrolytic cell was the same as in experiments 5 through 13. Intermittent square-wave electrolysis was performed at 1 Hz, 20% duty cycle, by programming a constant current supply (Kepco ATE-50M) at 10-A peak (±0.5%) driven by a function generator (BK Precision Dynascan model 3011). Data were recorded by the apparatus described for experiments 5 through 13. Since there was current only during the peak voltage interval of the cycle, P_{appl} was given by Eq. (25), and P_{cell} was given by Eq. (26).

LIGHT WATER CALORIMETRY RESULTS

Mills's theory[2] predicts that the exothermic catalytic reaction whereby the electrons of hydrogen atoms are each stimulated to relax to a lower energy level corresponding to a fractional quantum state by providing an energy hole resonant with this transition will occur during the electrolysis of K_2CO_3/light water solutions but will not occur during the electrolysis of Na_2CO_3/light water solutions. The results of the electrolysis with a nickel wire cathode at 83-mA constant current and heater run of K_2CO_3 appear in Fig. 7 and Table II. The heating coefficient of the heater run (calibration) was 41°C/W, whereas the heating coefficient of the electrolysis run was 87°C/W. The production of excess enthalpy is observed. The higher the heating coefficient is, the more heat is released in the process.

The results of the electrolysis of a K_2CO_3 electrolyte with a nickel cathode and a periodic square-wave having an offset voltage of 1.60 V, a peak voltage of 1.90 V, a peak constant current of 47.3 mA, a 36.0% duty cycle, and a frequency of 600 Hz appear in Fig. 8 and Table II. The output power was 16 times the ohmic input power.

The results of the electrolysis at 81-mA constant current and heater run of Na_2CO_3 appear in Fig. 9 and Table II. The heating coefficient of the electrolysis run was 47°C/W, whereas the heating coefficient of the heater run (calibration) was 46°C/W. The production of excess heat is not observed.

The data of the faradaic efficiency of the production of gas by a potassium cell and a control sodium cell appear in Table III.

Almost all electrolysis experiments will be similar to the case of Na_2CO_3. Only a few combinations of electrolytes and electrodes, such as the K_2CO_3 case, will yield excess heat.

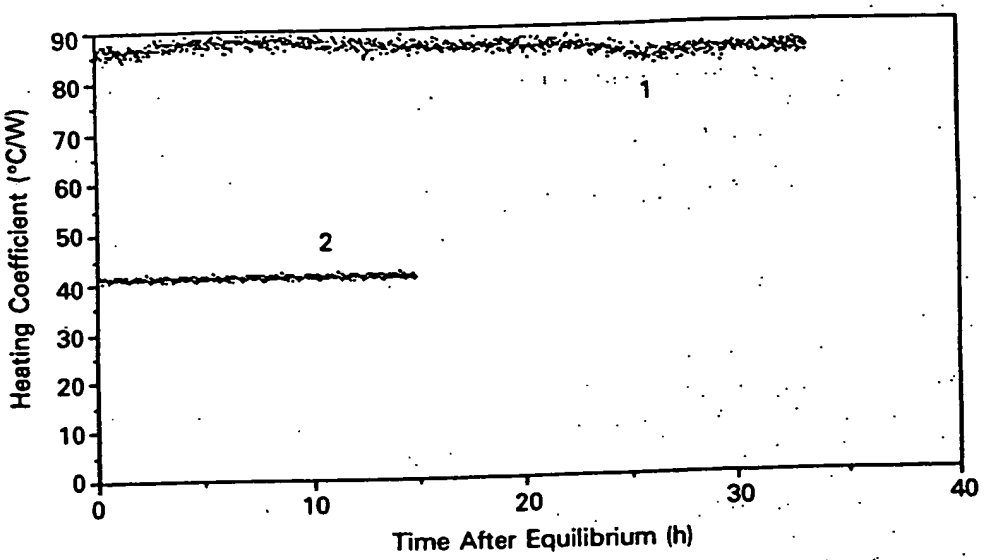

Fig. 7. Experiment 2: plot of the heating coefficients over time: (1) electrolysis with a nickel wire cathode at 0.083 A in K_2CO_3 and (2) resistor working in K_2CO_3.

TABLE II

Power Input and Output Parameters of Experiments 1 Through 14

Experiment Number	V (V)	Duty Cycle (%)	I (A)	VI Power (W)	$(V - 1.48)I$ Input Power (W)	Output Power (W)	Excess Power (W)	Output / Input (%)
1	3.05	100	0.083	0.253	0.130	0.275	0.145	212
2[a]	1.90	36	0.0473	0.032	0.007	0.114	0.107	1630
3	3.51	100	0.081	0.284	0.164	0.167	0.003	102
4	3.25	100	49.9	162	88.3	137	48.2	155
5[a]	4.13	3	101	12.5	8.03	31.0	21.5	386
6[a]	4.04	4	101	16.3	10.3	43.5	33.2	422
7[a]	4.00	5	102	20.4	12.9	54.7	41.8	424
8[a]	3.95	6	102	24.2	15.1	63.2	48.1	419
9[a]	3.89	7	101	27.5	17.0	70.0	53.0	412
10[a]	3.88	10	102	39.6	24.5	58.3	60.8	348
11[a]	3.88	15	101	58.8	36.4	105.5	69.1	290
12[a]	3.85	20	101	77.8	47.9	118.1	70.2	247
13[a]	3.83	25	101	96.7	59.3	135	75.7	228
14[a]	2.37	20	10.5	4.98	1.87	41.0	39.1	2193

[a]Output is greater than VI.

TABLE III

Faradaic Efficiency of Gas Production by a K_2CO_3 Cell and a Na_2CO_3 Control Cell

Electrolyte	Faraday's Gas (mmol)	Calculated Volume (ml)	Measured Volume (ml)	Efficiency (%)
0.57 M K_2CO_3	1.961	49.91	51.30	102.8
0.57 M Na_2CO_3	1.955	49.69	49.86	100.3

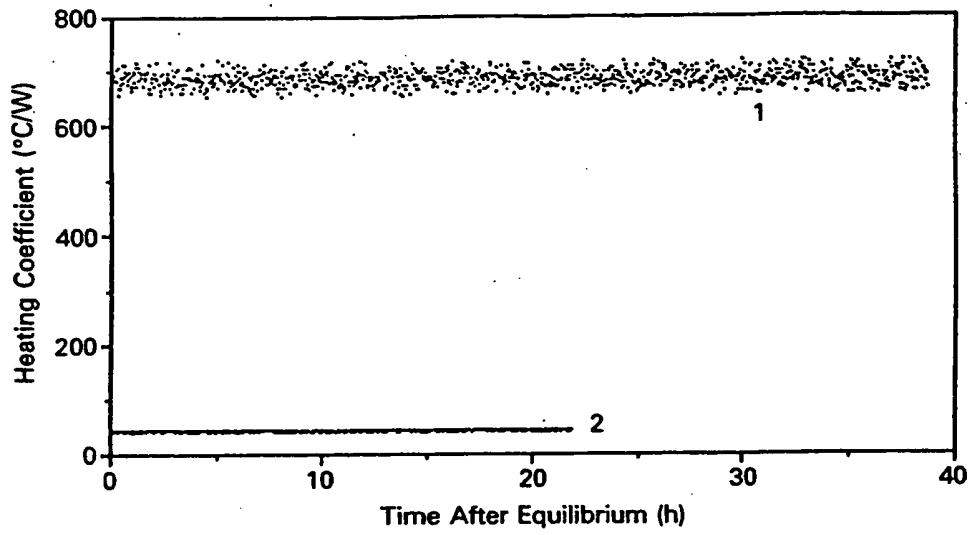

Fig. 8. Experiment 2: plot of the heating coefficients over time: (1) electrolysis with a nickel cathode and a periodic square wave having an offset voltage of 1.60 V, a peak voltage of 1.90 V, a peak constant current of 47.3 mA, a 36.0% duty cycle, and a frequency of 600 Hz in K_2CO_3 and (2) resistor working in K_2CO_3.

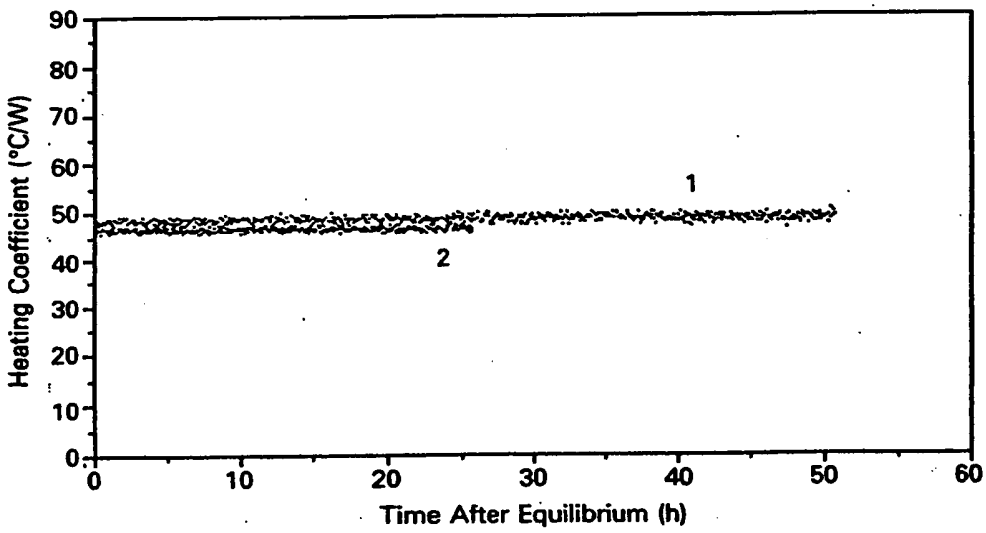

Fig. 9. Experiment 3: plot of the heating coefficients over time: (1) electrolysis at 0.081 A in Na_2CO_3 and (2) resistor working in Na_2CO_3.

Data from experiment 4 were recorded over a 29-day period. The voltage remained relatively constant at 2.35 V, and the electrolyte temperature was ~23°C above the temperature of the blank. The parameters at day 27 are given in Table II. The on-the-fly calibration curve of experiment 4 as well as the integral calibration curve for the matched blank cell are shown in Fig. 10.

The on-the-fly heating coefficient of the electrolytic cell was (0.17 ± 0.01°C/W). The intercept at zero input power for the integrally calibrated electrolytic cell was 8.2°C, which indicates 48.2 W of excess heat.

It was observed that gas sparging in the electrolytic cell provides sufficient mixing in the absence of stirring so that temperature gradients were not observed to within their detection limit (±0.1°C). The calibration (nonelectrolysis cell) was stirred at 250 rpm to compensate for the lack of stirring by gas sparging. It was determined that the stirring power increased the blank

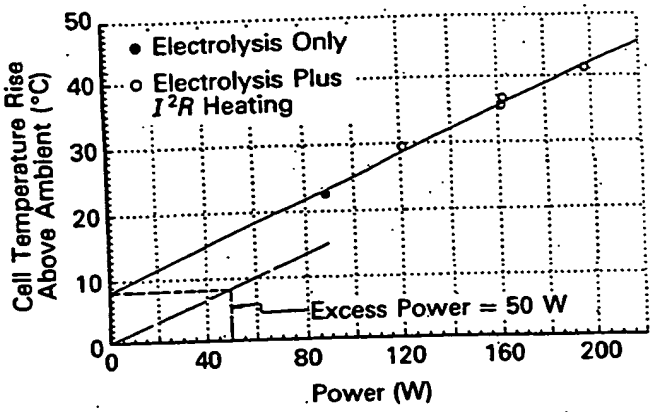

Fig. 10. A graphical determination of the excess power of experiment 4.

temperature 0.20°C above the ambient temperature, and this power was not subtracted from the blank temperature in the temperature measurements. Accounting for this temperature rise would increase the experimentally determined electrolytic cell excess energy by ~1.2 W.

From the condensed evolving water vapor, the evaporative losses from experiment 4 were measured to be 6.5 ml per 24 h, and 402 ml of water was added to the cell per 24 h to maintain a constant fill level. The volume consumed by Faraday losses is calculated to be 403 ml. Thus, the evaporative and Faraday losses equaled the maintenance water volume to within 1%.

Elemental analysis and scanning electron microscopy of metallurgical samples of the nickel cathode taken before operation and at day 56 of continuous operation were identical, indicating that the nickel cathode had not changed chemically or physically. Elemental analysis data of a sample of the nickel cathode taken at day 56 of continuous operation are shown in Table IV. Photomicrographs of a sample of the nickel cathode taken at day 56 of continuous operation are shown in Fig. 11.

The cell was disassembled and inspected after 23 days of continuous operation. This inspection showed no visible signs of a reaction between the electrodes and the electrolyte. The cell was reassembled, and it continued to operate with an excess power production of ~50 W for an additional 19 days, after which time the voltage and current parameters of experiment 5 were initiated.

TABLE IV

Chemical Analysis of the Nickel Wire of Experiment 4 After 56 Days of Operation

Mainly nickel
Trace (0.1 to 1.0%) copper
Slight trace (100 to 1000 ppm) magnesium
Very slight trace (10 to 100 ppm) aluminum and manganese
Very, very slight trace (<10 ppm) chromium, titanium, silver, tin, iron, silicon, boron, and phosphorus

TABLE V

Chemical Analysis of the Potassium Carbonate Electrolytic Solution of Experiment 4 After 42 Days of Operation

Flame emission spectrographic analysis
Mainly potassium
Slight trace (100 to 1000 ppm) sodium
Very slight trace (<10 ppm) magnesium
Specific gravity = 1.072
Concentration = 0.63 M K_2CO_3
Solution pH = 11.5

The pH, specific gravity, concentration of K_2CO_3, and elemental analysis of the electrolyte sample taken after 42 days of continuous operation were unchanged from the values obtained for the electrolyte sample before operation. These data are shown in Table V.

The results of the gas chromatographic analysis of the evolving electrolytic gases showed two-thirds hydrogen, one-third oxygen, and trace amounts of nitrogen. No significant quantities of CO or CO_2 were found, confirming that the K_2CO_3 electrolyte was not degraded during operation.

Measurements of neutrons were considered unnecessary since light water was used rather than deuterium oxide. Scintillation counter and photographic film measurements show no radiation above background was detected, indicating that nuclear reactions did not occur.

Data from experiments 5 through 13 were recorded over a 135-day period as the duty cycle was increased from 3 to 25%. The input and output powers are listed in Table II as a function of duty cycle. A comparison of cell temperature rise above ambient and power with the calibration curve is shown in Fig. 12. The comparison for experiment 9 shows ~53 W of excess energy at a 7% duty cycle. This corresponds to an output over input power ratio of ~4.12:1.

Data from experiment 14 were recorded over a 240-day period at an operating condition of 1 Hz, 10 A, and 20% duty cycle. Data for day 120 are recorded in Table II and show 41 W of output with an output-to-input ratio of ~22 assuming 100% Faraday efficiency. Actual Faraday efficiency at these low-current levels (2 A on average) has not been established. If the Faraday efficiency were zero (100% recombination), then the output-to-input ratio would be 8.2:1.

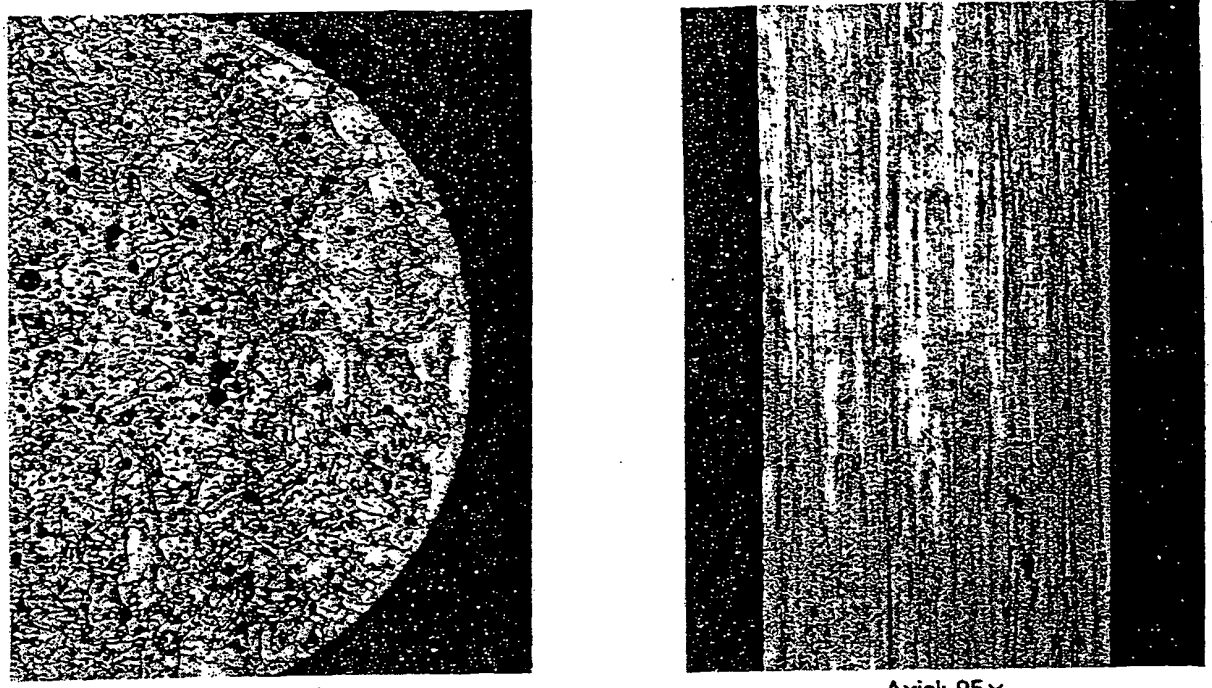

Fig. 11. Photomicrographs of metallurgical samples of the nickel cathode taken at day 56 of continuous operation.

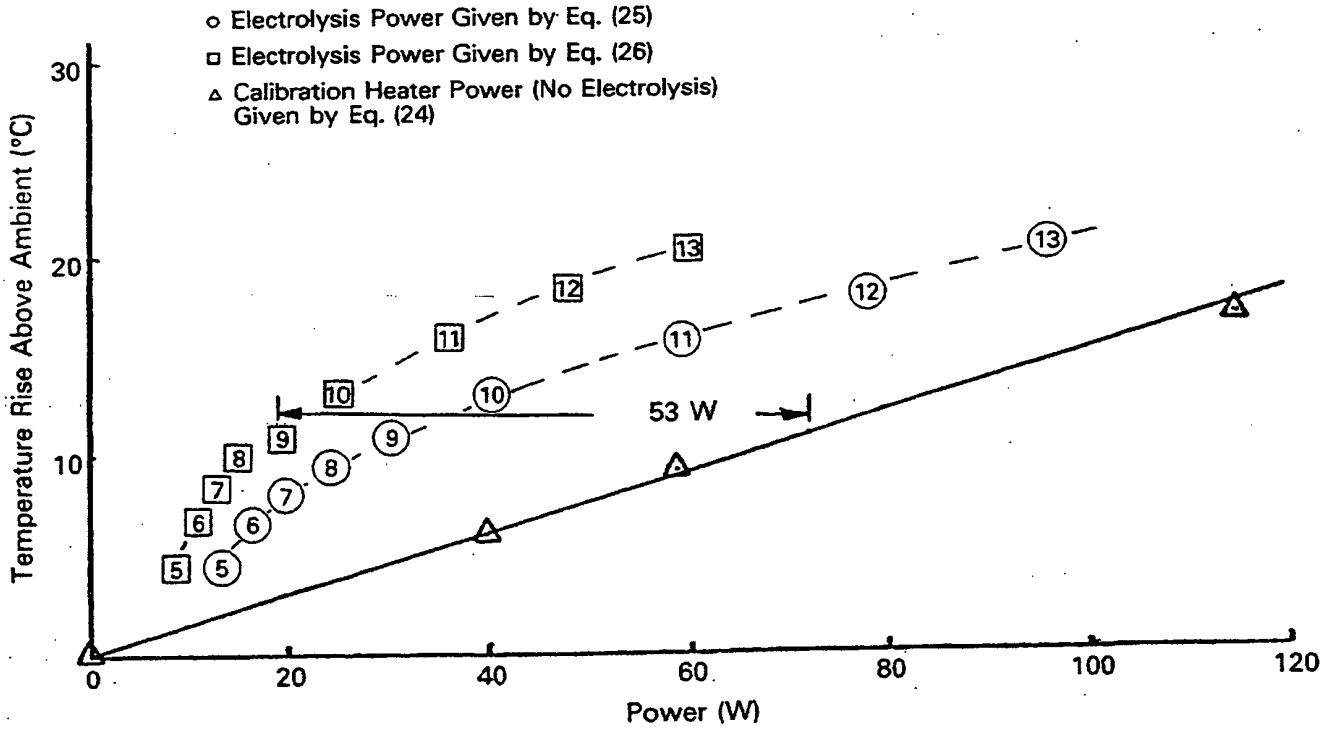

Fig. 12. Comparison between cell temperature rise above ambient for electrolysis power and for heater power for experiments 5 through 13.

EXPERIMENTAL IDENTIFICATION OF THE DIHYDRINO MOLECULE

The dihydrino molecules would be stable to combustion relative to molecular hydrogen, and the dihydrino molecule could be detected by mass spectroscopy with the presence of a $m/e = 2$ peak with a different branching ratio to form $m/e = 1$ relative to $m/e = 2$. To test this premise, we collected in an elastomer bladder 1650 ml of the electrolysis gases from experiment 14, which produced 39.1 W of excess power according to the exothermic reaction given by Eqs. (4), (5), and (6). The bladder contained a spark plug that was activated, causing an explosion of the gas contents. The volume of the bladder following combustion was 70 ml. Samples of the pre- and postcombustion electrolysis gases as well as hydrogen and water-saturated air were analyzed by mass spectroscopy.

The dihydrino molecule, H_2^*, has a higher ionization energy than H_2. Mass spectroscopy of the postcombustion electrolysis gas sample was performed whereby the intensity of the $m/e = 1$ and $m/e = 2$ peaks was recorded while the ionization potential of the mass spectrometer was varied.

The results of the mass spectroscopic analysis of gases evolved from experiment 14 before and after combustion are given in Table VI; of room air saturated with water, in Table VII; of the standard hydrogen sample, in Table VIII; and of the postcombustion electrolysis gas sample whereby the intensity of the $m/e = 1$ and $m/e = 2$ peaks was recorded while the ionization potential of the mass spectrometer was varied, in Table IX.

DISCUSSION

From Table VI, the $m/e = 18$ and $m/e = 32$ peak intensities, respectively, demonstrate that both the pre- and postcombustion electrolysis gas samples contained the same percentage of water vapor and of O_2. The predicted percentage for the precombustion electrolysis gas sample is one-third, as given by Faraday's law for the electrolysis of water. The oxygen signal for the postcombustion electrolysis gases is higher than can be due to atmospheric contamination.

From Table VI, the $m/e = 28$ peak intensity demonstrates that the pre- and postcombustion electrolysis gas samples contained the same percentage of nitrogen. The nitrogen was present in trace amounts in both gas samples as demonstrated by the $m/e = 28$ peak intensities from Table VI and the volume change with combustion. From the volume change, nitrogen represented <4% of the precombustion gas sample, and the $m/e = 28$ peak intensity of the postcombustion gas

TABLE VI

Mass Spectroscopic Analysis of Gases Evolved from the Cell of Experiment 14 Before and After Combustion ($IP = 70$ eV)

Mass/Charge (m/e)	Intensity of Precombustion Electrolysis Gases	Intensity of Postcombustion Electrolysis Gases
1	1.2×10^{-7}	0.40×10^{-7}
2	1.55×10^{-5}	0.55×10^{-7}
3	0.30×10^{-7}	
18	0.57×10^{-5}	0.55×10^{-5}
28	0.37×10^{-4}	0.90×10^{-4}
32	0.69×10^{-4}	0.65×10^{-4}
40	0.90×10^{-6}	0.40×10^{-5}
44	0.70×10^{-6}	0.12×10^{-5}

TABLE VII

Mass Spectroscopic Analysis of Room Air Saturated with Water ($IP = 70$ eV)

Mass/Charge (m/e)	Intensity ($\times 10^{-7}$)
1	0.24
2	0.040
18	43.0

TABLE VIII

Mass Spectroscopic Analysis of Hydrogen ($IP = 70$ eV)

Mass/Charge (m/e)	Intensity ($\times 10^{-7}$)
1	2.0
2	300.0
3 HD	0.12
3 H_3	2.0

TABLE IX

Mass Spectroscopic Analysis with Varying Ionization Potential of Gases Evolved from the Cell of Experiment 14 Following Combustion

Ionization Potential (eV)	Intensity of Signal Mass-to-Charge Ratio	
	($m/e = 1$)	($m/e = 2$)
20	0.007×10^{-8}	0.03×10^{-8}
70	1.8×10^{-8}	1.8×10^{-8}

sample was only a factor of 2.4 of that of the precombustion electrolysis gas sample. No hydrogen is anticipated following combustion.

The data are consistent with the remaining two-thirds of the postcombustion electrolysis gases comprising the dihydrino molecule, H_2^*, which does not undergo combustion with oxygen. The stoichiometric ratio of two-thirds H_2^* to one-third O_2 gives the correct mass balance. The $m/e = 2$ peak for the postcombustion electrolysis gases is ten times the intensity of the peak from water [given by the product of the ratio of $m/e = 2$ to $m/e = 18$ of the water-saturated air mass spectrum times the intensity of the $m/e = 18$ peak (H_2O) of the postcombustion electrolysis gas sample]. Thus, the $m/e = 2$ peak is assignable to H_2 or to H_2^*.

The assignment to H_2^* is made as follows. The $m/e = 1$ peak of the postcombustion electrolysis gas sample is significantly more intense than that predicted by production from water [given by the product of the ratio of $m/e = 1$ to $m/e = 18$ of the water-saturated air mass spectrum times the intensity of the $m/e = 18$ peak (H_2O) of the postcombustion gas sample]. The additional contribution to the $m/e = 1$ peak predicted with the assignment of the $m/e = 2$ peak to hydrogen (given by the product of the ratio of $m/e = 1$ to $m/e = 2$ of the hydrogen mass spectrum times the intensity of the $m/e = 2$ peak of the postcombustion electrolysis gas sample) is insufficient to explain the intensity of the $m/e = 1$ peak. Thus, the species giving rise to the $m/e = 2$ peak must have a different $m/e = 1$ to $m/e = 2$ production efficiency than H_2. Therefore, the $m/e = 2$ peak is assigned to H_2^*.

The dihydrino molecule, H_2^*, has a higher ionization energy than H_2. This was observed by measuring the intensity of the $m/e = 1$ and $m/e = 2$ peaks while the ionization potential of the mass spectrometer was varied. The ionization reaction of H_2 is

$$H_2(g) \rightarrow H_2(g)^+ + e^- \quad IE = 15.46 \text{ eV} . \qquad (29)$$

The ionization energies of water are 12.61, 14.8, 18.8, and 32 eV. The data of Table IX demonstrate that no $m/e = 2$ peak is present at an ionization potential above the threshold for the ionization of molecular hydrogen, but a $m/e = 2$ peak that is too intense to be attributed to water ionization is present at a significantly higher ionization potential. The data are consistent with the assignment of $m/e = 2$ to H_2^*, the dihydrino molecule.

CONCLUSION

We review and present three sets of heat production and product identification data including the work of HydroCatalysis Power Corporation (experiments 1, 2, and 3) and Thermacore, Inc. (experiments 4 through 14). We report here experimental evidence supporting the HPC theory that an exothermic reaction occurs wherein the electrons of hydrogen and deuterium atoms are each stimulated to relax to a quantized potential energy level below that of the ground state via electrochemical reactants K^+ and K^+; Pd^{2+} and Li^+; or Pd and O_2 of redox energy resonant with the energy hole that stimulates this transition. Calorimetry of pulsed current and continuous electrolysis of aqueous potassium carbonate (K^+/K^+ electrocatalytic couple) at a nickel cathode was performed. The excess output power of 41 W exceeded the total input power given by the product of the electrolysis voltage and current by a factor of >8. The product of the exothermic reaction is atoms having electrons each of energy below the ground state, and they are predicted to form molecules. The predicted molecules were identified by their lack of reactivity with oxygen, by separation from molecular deuterium by cryofiltration, and by mass spectroscopic analysis.

The combustion of the gases evolved during the electrolysis of a K_2CO_3/light water electrolyte (K^+/K^+ electrocatalytic couple) with a nickel cathode was incomplete. The mass spectroscopic analysis of uncombusted gases demonstrated that the species predominantly giving rise to the $m/e = 2$ peak must have a different $m/e = 1$ to $m/e = 2$ production efficiency than hydrogen. The further mass spectroscopic analysis of the $m/e = 2$ peak of the uncombusted gas demonstrated that the dihydrino molecule, H_2^*, has a higher ionization energy than H_2.

The mass spectroscopic analysis of the cryofiltered gases evolved during the electrolysis of a heavy water LiOD electrolyte (Pd^{2+}/Li^+ electrocatalytic couple) with a palladium cathode demonstrated that the dideutrino molecule, D_2^*, has a higher ionization energy than D_2.

Palladium sheets coated on one side with a hydrogen-impermeable gold layer and on the other surface with an oxide coat (MnO_x, AlO_x, or SiO_x) were loaded with deuterium or hydrogen. Heat was observed from light and heavy hydrogen only when the mixed oxide coat was present (Pd/O_2 electrocatalytic couple). The high-resolution (0.001 amu) quadrupole mass spectroscopic analysis of the gases released when a current was applied to a deuterium-loaded (99.9%), MnO_x-coated palladium sheet indicate the presence of a large shoulder on the D_2 peak that is due to the dideutrino molecule, D_2^*.

Further experiments are planned to demonstrate that this lower energy form of hydrogen is the product of heat-producing cells. Following cryofiltration of the electrolysis gases, the dihydrino molecule is distinguished from normal molecular hydrogen by mass spectroscopy. The branching ratio to form $m/e = 1$ relative to $m/e = 2$ that is observed for the dihydrino molecule is different from the ratio that is observed for normal molecular hydrogen. Mass spectroscopy further distinguishes a sample containing dihydrino molecules from a sample containing H_2 by showing a different ion production efficiency as a function of ionization potential and a different ion production efficiency at a

given ionization potential for the two samples. High-resolution mass spectroscopy shows two peaks for a mixture of H_2 and H_2^*.

ACKNOWLEDGMENTS

Special thanks to J. Farrell for technical support, papers, discussions, and review of this manuscript and to D. Parees, of Air Products Corporation, who performed the mass spectroscopy.

REFERENCES

1. H. A. HAUS, "On the Radiation from Point Charges," *Am. J. Phys.*, 54, 1126 (1986).

2. R. MILLS, *Unification of Spacetime, the Forces, Matter, and Energy*, Technomics Publishing Company, Lancaster, Pennsylvania (1992).

3. R. NIEMINEN, "Atoms Band Together," *Nature*, 365, 289 (1992).

4. J. FARRELL, W. GOOD, and R. MILLS, "An Alternative Explanation of Extreme Ultraviolet Emissions from Dark Matter," submitted to *Astrophys. Lett. Communications* (1993).

5. M. H. MILES, B. F. BUSH, G. S. OSTROM, and J. J. LAGOWSKI, "Helium Production During the Electrolysis of D_2O in Cold Fusion Experiments," *J. Electroanal. Chem.*, 304, 271 (1991).

6. R. DAGANL, "New Evidence Claimed for Nuclear Process in Cold Fusion," *Chem. Eng. News*, 31 (Apr. 1, 1991).

7. M. H. MILES, B. F. BUSH, G. S. OSTROM, and J. J. LAGOWSKI, "Heat and Helium Production in Cold Fusion Experiments," *Proc. Conf. The Science of Cold Fusion*, Como, Italy, June 29–July 4, 1991, p. 363, T. BRESSANI, E. DEL GIUDICE, and G. PREPARATA, Eds., SIF (1991).

8. M. H. MILES, R. A. HOLLINS, B. F. BUSH, J. J. LAGOWSKI, and R. E. MILES, "Correlation of Excess Power and Helium Production During D_2O and H_2O Electrolysis Using Palladium Cathodes," *J. Electroanal. Chem.*, 346, 99 (1993).

9. C. C. CHIEN, D. HODKO, Z. MINEVSKI, and J. BOCKRIS, "On an Electrode Producing Massive Quantities of Tritium and Helium," *J. Electroanal. Chem.*, 338, 189 (1992).

10. B. F. BUSH, Department of Chemistry, University of Texas, Austin, Personal Communication (1993).

11. S. JONES, Newsgroups: sci.physics.fusion (Mar. 3, 1993).

12. M. H. MILES and B. F. BUSH, "Search for Anomalous Effects Involving Excess Power and Helium During D_2O Electrolysis Using Palladium Cathodes," *Proc. 3rd Int. Conf. Cold Fusion*, Nagoya, Japan, October 21–25, 1992, p. 189.

13. B. REES, "Cold Fusion: What Do We Know? What Do We Think?" *J. Fusion Energy*, 10, *1*, 111 (1991).

14. E. YAMAGUCHI and T. NISHIOKA, "Direct Evidence for Nuclear Fusion Reactions in Deuterated Palladium," *Proc. 3rd Int. Conf. Cold Fusion*, Nagoya, Japan, October 21–25, 1992.

15. E. YAMAGUCHI and T. NISHIOKA, "Helium-4 Production from Deuterated Palladium at Low Energies," NTT Basic Research Laboratories and IMRA Europe S.A., Personal Communication (1992).